# Influence of proximity effects in electron-beam lithography on the optical properties of planar photonic-crystal waveguides

R. Wüest,[a] F. Robin,[b] P. Strasser, and H. Jäckel
*Communication Photonics Group, Electronics Laboratory (IfE), ETH Zurich, 8092 Zurich, Switzerland*

D. Erni
*General and Theoretical Electrical Engineering (ATE), Faculty of Engineering, University of Duisburg-Essen, 47048 Duisburg, Germany*

(Received 13 June 2007; accepted 3 September 2007; published online 29 October 2007)

To measure the influence of proximity effects in electron-beam lithography on the optical properties of planar photonic crystal (PPC) waveguides we propose a PPC structure called the "PECmeter." The PECmeter consists of nearly identical PPC waveguides which only differ in the number of rows of holes along the waveguide. The difference in the number of rows does not influence the modal properties directly but changes the diameter of the holes neighboring the waveguide through the proximity effect. The operation principle of the PECmeter is demonstrated using energy-intensity simulations of a W3 waveguide (three missing rows of holes) mini stop band. The principle is confirmed experimentally with structures fabricated in the InP-based material system and measured by the end-fire transmission technique. The results clearly show that the application of proximity-effect correction (PEC) is crucial for the fabrication of PPC waveguides. We demonstrate that when using the midpoint-equalization PEC method a near-to-perfect correction with sub-nm hole-radius uniformity can be achieved. We show the PECmeter to be sensitive enough to detect hole-radius changes as small as $\Delta R = 0.4$ nm. © *2007 American Institute of Physics*.
[DOI: 10.1063/1.2801023]

## I. INTRODUCTION

Planar photonic crystal (PPC) devices are excellent candidates for a range of applications due to their compact light guiding mechanism and highly tunable optical properties.[1] Examples include waveguides with radically reduced group velocities,[2] high-quality resonators with small mode volumes,[3] and miniaturized wavelength multiplexing devices.[4] Such structures mostly rely on the customizable dispersion relation of PPC waveguides and consequently on the radius of the holes which are adjacent to the waveguide.

The fabrication process, which should provide sufficient accuracy in the hole diameters, often consists of an initial electron-beam lithography (EBL) step and a subsequent pattern transfer with a plasma etching method. EBL, as the initial patterning step, is decisive for the achievable accuracy of the resulting structure. In EBL, proximity effects due to electrons backscattering are the predominant factors which limit the achievable structural accuracy. Consequently, proximity-effect correction (PEC) methods are widely used in PPC fabrication.[5] Challenging—for current nanofabrication in general and PEC methods in particular—is the required accuracy on the nanometer level combined with the large variations in structural density of PPC devices.

The straightforward way to assess the performance of PEC methods is the analysis of scanning electron microscopy (SEM) micrographs as it is often found in literature.[5–10] Nevertheless, the final benchmark of PEC methods in PPC fabrication is the control and reproducibility of the optical properties of fabricated devices. Few investigations are found in literature, which show the influence of proximity effects on optical properties of PPC devices.[11,12] None of them provides a quantitative description of the connection between proximity effects and optical measurements, which is the objective of this work.

We will propose in this article a technique coined the "PECmeter," which allows us to measure with an unprecedented accuracy the impact of EBL proximity effects on the optical properties of PPC waveguides. Further, the PECmeter offers a highly sensitive means to check the quality of the applied PEC and the accuracy of the proximity parameters. Indeed, their experimental determination is influenced by insulating masking layers which induce charging effects, while Monte-Carlo-based modeling techniques may become unreliable for complex multilayer structures. In addition, energy-intensity distribution (EID) simulations of the EBL process[9] will be used to obtain a quantitative prediction of the associated spectral shifts of distinct waveguide features.

This article is organized as follows: After explaining in Sec. II the PECmeter concept, we will use in Sec. III EID simulations to predict the impact of proximity effects on the spectral position of the W3 ministop band (MSB)—which proves a better suited indicator than optical features of W1 waveguides. The fabrication of the PECmeter and the analysis of SEM micrographs will be shortly discussed in Sec. IV, followed by end-fire transmission measurements of the waveguides. Results from the optical measurements and plane-wave simulations of the modal dispersion relation using hole diameters from EID simulations and SEM micrograph analysis are compared in Sec. VI.

[a]Electronic mail: wueest@ife.ee.ethz.ch
[b]Electronic mail: robin@ife.ee.ethz.ch

 

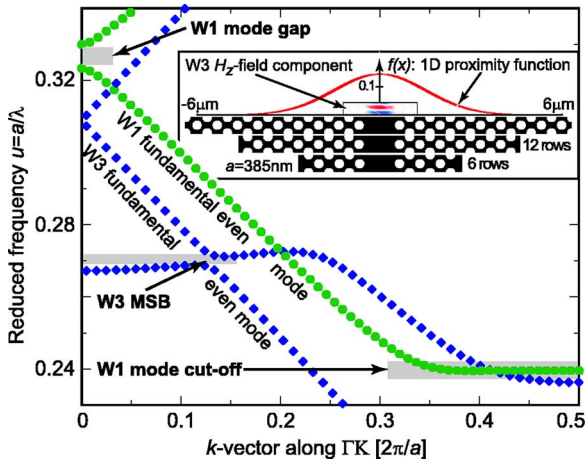


FIG. 1. (Color online) Waveguide dispersion of the W1 and W3 fundamental modes. Three optical features (W1 mode gap, W3 mini stop band, and W1 mode cutoff), whose spectral location is sensitive on the hole diameters of the adjacent rows are shown. Inset: lateral extent of the $H_z$-field component of the W3 fundamental mode and of the 1D EBL proximity function of the backscattered electrons with $\eta=1.17$ and $\beta=2.12$ $\mu$m, compared to W3 waveguides with 6, 12, and 18 adjacent rows of holes.

## II. PECMETER CONCEPT

In principle, any spectrally distinct feature in the optical spectrum of a PPC structure depending on the size of adjacent holes, e.g., a cavity resonance frequency, could be used to measure the impact of proximity effects and of the correction technique. It is, however, advantageous not to depend on the fine details of individual holes which could also be altered by local fluctuations of the etching processes. More suitable are global optical features which are determined by a large number of holes as in PPC waveguides. Waveguides are further advantageous as they can easily be modeled with a plane wave expansion method such as the freely available MIT Photonics Bands (MPB) package.[13,14] This allows for a comparison between (i) optical transmission measurements, (ii) dispersion relations computed using hole diameters from SEM micrographs, and (iii) hole diameters from EID simulations.[9] Finally, the EID simulations can be combined with MPB to predict the shift of the waveguide feature due to proximity effects.

In the dispersion diagram of Fig. 1 the fundamental even modes of W1 (one missing row of holes along the $\Gamma K$-direction) and W3 waveguides (three missing rows of holes) are displayed. They include three distinct optical features which lend themselves to spectral-shift measurements: the W1 mode gap at the Brioullin zone boundary, the W3 MSB and the W1 mode cutoff. The W3 MSB originates from the avoided crossing due to mode coupling of the fundamental mode with a higher order mode. It can also be interpreted as the Bragg stop gap which is associated to the corrugation introduced by the row of holes adjacent to the W3 waveguide. The spectral position of all three features depends mainly on the size of the adjacent rows of holes with a sensitivity summarized in Table I together with the range of fill ratios for which they are located within the photonic band gap. An estimate of their spectral width is given as well. The values in Table I were obtained from two-dimensional (2D) MPB simulations relying on the effective-index method. These computations show a sufficient degree of accuracy for the InP/InGaAsP/InP low vertical index contrast slab waveguide investigated here.[15] The suitability of a spectral feature to quantify the impact of proximity effects depends on the spectral resolution with which it can be located and its sensitivity toward changes in hole diameters. The results of the sensitivity analysis show that the W1 mode cutoff exhibits the largest sensitivity to hole-size variations. The W1 mode cutoff is, however, hard to locate in InP-based substrate-type PPCs because of difficulties to couple light into the waveguide within the slow-light region[16] and due to excessive losses of the transversely extended mode. The W1 mode gap on the other hand is very distinct and can be located accurately, but it does not shift much when changing hole diameters. The W3 MSB presents a compromise, both regarding spectral width and sensitivity and offers the advantage that it is observable over the full range of fill ratios. Additionally, when coupling light from a deeply etched trench waveguide, the fundamental mode of the W3 waveguide is predominantly excited due to the good mode profile overlap.

TABLE I. Optical waveguide features are shown in Fig. 1 with spectral sensitivities to a uniform change in hole diameters, the suitable range of fill ratios and the expected spectral width for InP-based substrate type PPCs. Numbers are obtained from 2D MPB simulations with $n_{\text{eff}}=3.26$ and for wavelengths around $\lambda=1500$ nm.

| Characteristic | Sensitivity $\Delta\lambda$ per $\Delta R/a=0.01$ | Fill ratio range | Spectral width |
|---|---|---|---|
| W1 mode gap | 6.1 nm | $R/a\geq 0.34$ | $\approx$15 nm |
| W3 MSB | 10.5 nm | Full range | 30–50 nm |
| W1 mode cutoff | 16.2 nm | $R/a<0.37$ | hard to locate |

To estimate the sensitivity of the PECmeter toward hole radius changes, we focus on the MSB of a W3 waveguide with a lattice constant of $a=400$ nm, the spectral location thereof can be measured with an accuracy of $\Delta\lambda=1$ nm (see Sec. V). From Table I we see that the MSB spectral location is therefore sensitive to hole radius changes of $\Delta R=0.4$ nm. This should be compared to techniques using SEM micrographs for which best reported values are on the order of 1–2 nm, limited by the diameter of the electron beam.[17]

The PECmeter consists of nearly identical waveguides which only differ in the number of rows of holes on each side of the waveguide, in our case 6, 12, or 18 rows, as shown in Figs. 4(b). These three waveguides are located close to each other and are EBL written in close sequence to minimize parasitic beam drift or current fluctuations. Because the remaining fabrication steps are of parallel nature and do not introduce any additional differences between the waveguides, any optical discrepancy must be attributed to the different number of rows of holes adjacent to the waveguides and consequently to proximity effects. We will now explain the PECmeter concept and how proximity effects give rise to detectable changes in the optical spectrum.

The optical fields of even PPC waveguide modes are concentrated in the center of the waveguide. Representative for the field distribution in the W3 waveguide, the $H_z$ component of the fundamental mode is shown in the inset of Fig.

1. Therefore, mainly holes located adjacent to the waveguide influence its properties significantly such as the frequency position of mode gaps or MSBs. Rows of holes located further away do not induce any substantial MSB shift. For instance, 2D MPB simulations of a W3 waveguide revealed that changing the radius of the holes in the seventh row from $R/a=0.1$ to $R/a=0.5$ shifts the spectral location of the W3 MSB by less than $\Delta u \leq 2\times 10^{-5}$, or $\Delta\lambda \leq 0.1$ nm at a wavelength $\lambda=1500$ nm. This shift is smaller than the tolerance with which the W3 MSB can be spectrally resolved in our measurements.

EBL proximity effects, on the other hand, exhibit a characteristic length $\beta$ of the electrons backscattering which is $\approx 2$ $\mu$m for InP substrates at 30 kV. The value of $\beta$ depends on the substrate material and the acceleration voltage. The one-dimensional (1D) proximity function $f(x)$ is given by

$$f(x)=\frac{1}{\sqrt{\pi}(1+\eta)}\left(\frac{1}{\alpha}e^{-x^2/\alpha^2}+\frac{\eta}{\beta}e^{-x^2/\beta^2}\right). \quad (1)$$

It represents the transverse proximity effect of an infinite line in $y$-direction. In this equation, forward-scattering effects are represented by the first Gaussian term with width $\alpha$. Energy deposition by backscattered electrons is modeled by the second Gaussian term of width $\beta$ which is drawn as well in the inset of Fig. 1. $\eta$ denotes the backscattering efficiency. Because the optical interaction length is significantly shorter than the backscatter range (see inset of Fig. 1), additional holes beyond the sixth row only affect the optical mode indirectly through a slight alteration of the diameter of the holes adjacent to the waveguide.

PECmeter devices without PEC and with the midpoint-equalization PEC method[9,18] were fabricated, measured and compared to EID simulations[9] and MPB simulations. In the next section we will qualitatively assess the PECmeters and provide an estimate of the expected effects.

## III. ASSESSMENT OF THE PECMETER WITH EID SIMULATIONS

For EID simulations[9] the planar distribution of the energy deposited in the resist is calculated by summing up the contribution of each exposed pixel which is described by the 2D proximity function $f(r)$ as given in

$$f(r)=\frac{1}{\pi(1+\eta)}\left(\frac{1}{\alpha^2}e^{-x^2/\alpha^2}+\frac{\eta}{\beta^2}e^{-x^2/\beta^2}\right), \quad (2)$$

where $r$ denotes the radial distance and $\alpha$, $\beta$, and $\eta$ are the proximity parameters described earlier. EID simulations are a powerful tool to quantitatively predict the influence of proximity effects on hole diameters. Due to the lack of suitable models for the plasma etching steps involved in the holes fabrication, only a relative quantitative prediction of final hole diameters is possible. Nevertheless, as for the three W3 waveguides all parameters are kept constant except for the proximity effect-induced background dose, we expect EID simulations to provide a meaningful estimate of the relative hole-diameter change. Based on the extracted hole diameters, 2D MPB simulations can be used to estimate the expected relative MSB spectral shifts.

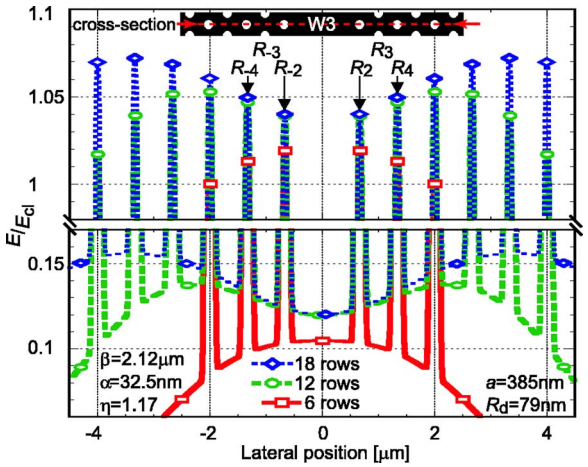


FIG. 2. (Color online) Cross sections through EID simulations when no PEC is applied ($D/D_{cl}=2$) for W3 waveguides with 6 (red rectangles), 12 (green ellipses), and 18 (blue diamonds) rows of holes on each side. Hole radii for the 3 adjacent rows on each side of the waveguide ($R_{-4}$, $R_{-3}$, $R_{-2}$, $R_2$, $R_3$, $R_4$) are extracted from binary images (see inset at the top) obtained at a development energy of $E/E_{cl}=1/1.53$.[9]

The EID simulations were performed with the parameters given in Fig. 2. For the hole-radius extraction, only the central part ($20a$) of the overall $60a$ long simulated waveguide was used so that it can be considered to be longitudinally invariant. Cross sections through EID simulations of W3 waveguides with 6, 12, and 18 rows on each side are depicted in Fig. 2 for the uncorrected case. The bottom and top parts show details of the background energy distribution and the energy-cones maxima of the exposed holes, respectively. The hole size after development is well reproduced by the area which receives more energy than the threshold $E/E_{cl}=0.65$. This development threshold has been determined through measurements published elsewhere.[9] Because the slope of the energy cones is constant and is related to $\alpha$, the height of the background and the energy-cones maxima are related to the hole diameters. Consequently, a lower background and energy-cone maximum indicate a reduced diameter. In the bottom part of Fig. 2 it can be seen that the energy background in the center of the waveguide for the six-row PECmeter is significantly lower than for 12- and 18-row waveguides, between which no significant difference is visible. Accordingly, the energy cones for the rows adjacent to the waveguide are of almost identical height for the PECmeters with 12 and 18 rows but are reduced for PECmeters with 6 rows. From this observation we expect a MSB spectral shift for waveguides with 6 and 12 rows, but only a marginal shift between 12 and 18 rows. The 1D proximity function confirms this observation as it is close to zero beyond the twelfth row as can be seen in the inset of Fig. 1. Therefore, according to the reciprocity principle,[19] the dose applied to rows 13–18 influences the background energy in the center of the waveguide only marginally.

The hole radii after development were extracted from the EID simulations. The radii after etching were then obtained with the help of a formula fitted to experimental data: the final hole radius in InP $R_f$ (nm) is given by $R_f=1.1\cdot R_d+38$ according to an evaluation of SEM micrographs where $R_d$ denotes the design radius. The estimated diameters of the

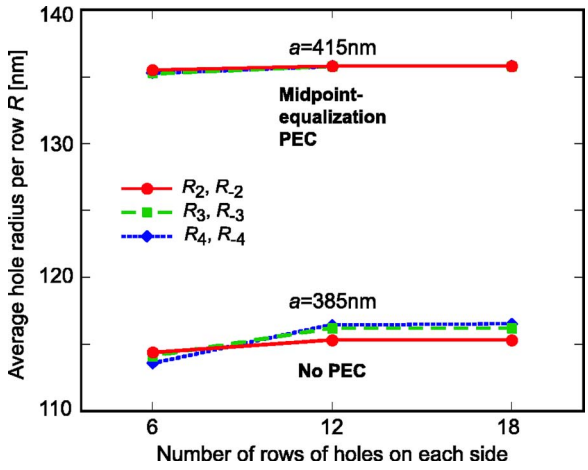


FIG. 3. (Color online) Hole radii extracted from EID simulations for the uncorrected and the midpoint-equalization corrected structures. The predicted final hole radii $R$ after etching were used to simulate the expected spectral shift of the W3 MSB with 2D MPB.

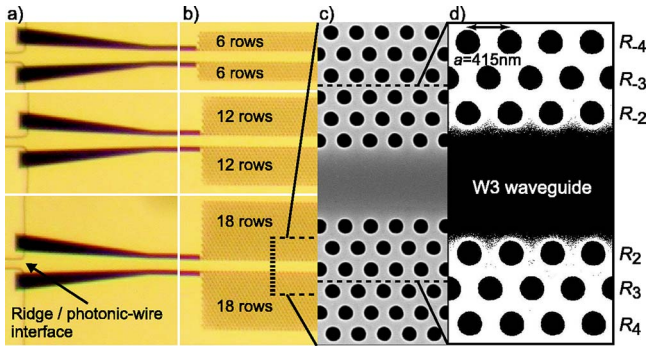


FIG. 4. (Color online) Fabrication and analysis of PECmeters: (a) optical microscope images of the access-ridge to trench-waveguide interface and (b) of three W3 waveguides (length 180$a$ with 6, 12, and 18 rows on each side, (c) high resolution SEM micrograph (4 nm/pixel) of the central region of the waveguide, and (d) binary image of the central 6 rows obtained by thresholding the SEM micrograph.

fabricated holes adjacent to the waveguide are shown in Fig. 3. It can be seen that when no PEC is applied, holes enlarge when increasing the number of rows, with the effect being more pronounced for holes from rows $R_3$ and $R_4$. For the midpoint-equalization PEC, a near-to-perfect correction is obtained. The residual minute enlargement upon increasing the total number of rows from 6 to 12 is due to tiny imperfections in the correction of the small disks used to define the PhC holes.[9]

The extracted hole diameters were used as input parameters for 2D MPB simulations. The resulting absolute spectral locations of the MSBs cannot be compared quantitatively to fabricated structures because plasma-etching effects were only partly taken into account and may differ when changing the lattice constant or the design radius due to reactive ion etching lag. Nevertheless, the simulated relative spectral shifts can be compared with the measured shifts, because structural alterations are expected to be identical for all waveguides which are EBL written, developed and plasma-etched simultaneously. To the first order, MSB shifts are therefore attributed to proximity effects. The computed MSB shifts according to EID simulations are shown in Fig. 9(b) as green diamonds. A significant shift is predicted in the uncorrected case for designs with 6 and 12 rows whereas for the midpoint-equalization PEC, the resulting spectral shift is very close to zero. For both corrected and uncorrected cases, no MSB shift is computed between waveguides with 12 and 18 rows.

## IV. FABRICATION OF PECMETERS AND ANALYSIS OF SEM MICROGRAPHS

PECmeters were fabricated without correction and with the midpoint-equalization PEC,[18] for two different lattice constants $a=385$ and 415 nm and a waveguide length of 180$a$. The fabrication process is published elsewhere.[20] Briefly, it consists of three main steps:

1. Photolithography and subsequent lift-off process of Au markers serving as alignment marks for the subsequent EBL and optical lithography steps.
2. EBL and plasma etching of deeply etched PPC and trench waveguides.[21,22]
3. Optical lithography and plasma etching of long shallow-etched access ridge waveguides suitable for fiber-optic coupling.

The single-mode ridge waveguides served to access the W3 waveguides from the chip facets. Figures 4(a) and 4(b) present an overview of the fabricated PECmeters. The in-coupling from the ridge waveguides to the trench waveguides is visible in Fig. 4(a) and the interface between the trench waveguide and the W3 waveguide is depicted in Fig. 4(b). The three structures with 6, 12 and 18 rows were sequentially exposed with EBL for each period. In this way, parasitic differences between the PECmeters which could be caused by a drift of the EBL beam current or focus can be minimized. A high resolution SEM micrograph taken from the central part of one of the structures is shown in Fig. 4(c). Such micrographs were recorded for all waveguides and analyzed using image processing techniques to extract the diameters of individual holes [see Fig. 4(d)].[9] Eighteen to twenty holes were analyzed per row to ensure an accurate determination of the average hole radii.

Results from the extraction procedure are shown in Fig. 5. The structures without PEC show a distinct increase of the central hole diameters when the number of rows is increased from 6 to 12 but only a marginal change between 12 and 18 rows structures. For the midpoint-equalization PEC, extracted radii are the same for all structures within the extraction tolerance of a few nanometers. This confirms the excellent patterning quality which can be achieved with this PEC method.

The extracted hole radii were used as input parameters for 2D MPB simulations, from which the position of the W3 MSBs and their shifts for 6, 12, and 18 rows were calculated as shown in Fig. 9. Such simulations can be compared to the MSB positions measured from optical transmission spectra as will be discussed in Sec. VI.

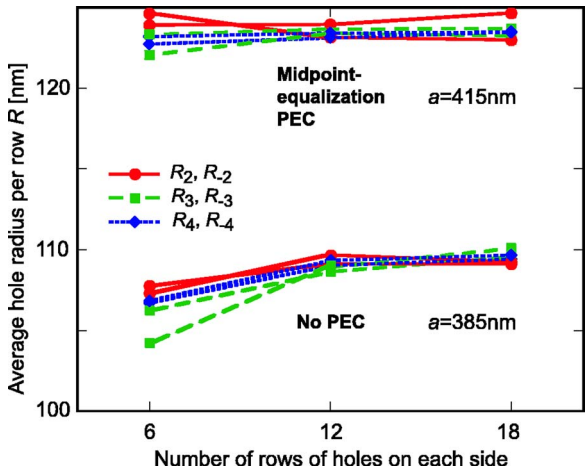


FIG. 5. (Color online) Hole-radius extraction from SEM micrographs. The measured radii $R$ were used to simulate the expected spectral location of the W3 MSB with 2D MPB.

## V. MEASUREMENT AND DATA ANALYSIS

Transmission measurements were performed on the PECmeter structures using a port-to-port end-fire setup shown in Fig. 6. Spectrally distinct optical features naturally lend themselves to investigations with the end-fire method, as no reproducibility on the absolute transmitted power is required and a large number of structures has to be measured (10–20) due to the requirements of lithographic tuning.[23]

In order to reliably determine the spectral position of the MSB, transmission spectra were recorded with a fine resolution ($\Delta\lambda=0.1$ nm) over a wavelength range sufficiently large to allow for a normalization of the transmitted power outside the MSB. The MSB of the PECmeters without PEC happen to fit only partly within the wavelength range of our lasers for $a=385$ nm as shown in Fig. 7(a). Nevertheless, proximity effects clearly result in a shift of the MSB toward lower wavelengths by roughly 10 nm when the number of rows is increased. On the other hand, PECmeter structures corrected with the midpoint-equalization method, show insignificant shifts, below the W3 MSB position extraction tolerance of $\Delta\lambda=1$ nm as can be seen in Fig. 7(b). These results are in full qualitative agreement, both with the EID simulations and the SEM micrographs analysis.

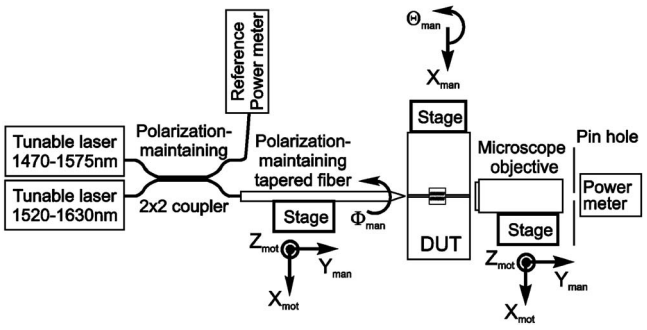


FIG. 6. Schematic of the end-fire setup used for the transmision measurements. The device-under-test (DUT) consists of 1 mm long ridge access waveguides which guide the light from the cleaved chip facets to the W3 PPC waveguide (~100 $\mu$m long). The light from the two tunable laser sources is coupled from a polarization-maintaining lensed fiber to the ridge waveguides and collected on the other side with a microscope objective.

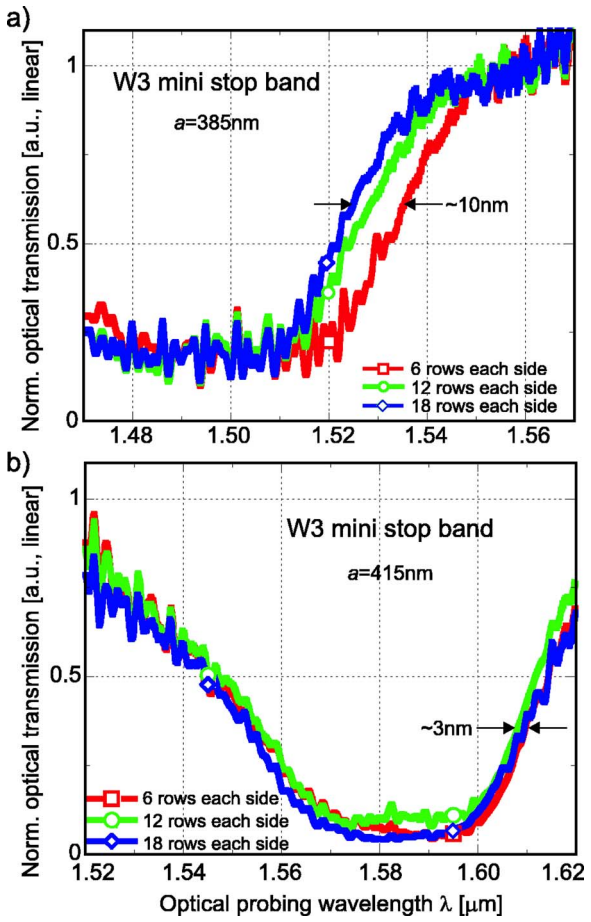


FIG. 7. (Color online) Normalized optical transmission around the MSB of W3 waveguides with 6 (red square), 12 (green circle), and 18 (blue diamond) rows of holes on each side: (a) no PEC and (b) midpoint-equalization PEC. The optical transmission was normalized to one outside the MSB, around $\lambda=1.56$ and 1.5 $\mu$m for (a) and (b), respectively.

In Fig. 8(a) the simulated dispersion relation of the W3 even mode with hole diameters extracted from the SEM micrographs is shown for a midpoint-equalization corrected PECmeter (18 rows, $a=415$ nm). Arrows indicate the edges of the MSB. Figure 8(b) shows the measured and normalized optical transmission for the same structure as in Fig. 8(a). Red dots display the raw data while the solid green line represents the same data set after application of a 1 nm moving average filter to suppress the Fabry-Perot interference fringes from the cleaved facets. Both flanks of the MSB were fitted individually with a sixth-order polynomial. The polynomial function crossing with the −5 dB level, laying conveniently below the interference fringes, was used to indicate the experimental ministop band edge. This method allows for the determination of the MSB edges with a ±1 nm tolerance as estimated from the measurement-data scattering around the polynomial fitting curve, which translates in a reduced-frequency error bar of $\Delta u=3.3\times10^{-4}$. The difference in the measured and simulated absolute positions of the MSB arises from the 2D MPB simulations which do not account for material and waveguide dispersion[24] and for noncylindrical

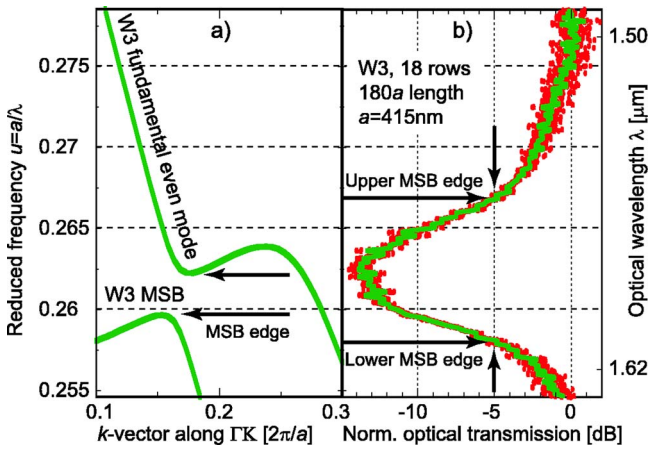


FIG. 8. (Color online) (a) Dispersion relation of the W3 waveguide fundamental even mode around the MSB simulated with 2D MPB with hole radii determined from SEM micrographs (18 rows, $a=415$ nm, midpoint-equalization PEC). (b) Measured transmitted power of the same waveguide as simulated in (a) normalized to the transmission at short wavelengths. Red dots: raw data, green line: smoothed data. Lower and upper spectral positions of the MSB are indicated in both cases with arrows. The vertical axes for both simulation and measurement are expressed in reduced frequency. The wavelength scale on the right-hand side is a guide for the eyes only.

hole shapes.[22] However, for the purpose of this study, only the relative shift of the consistently determined MSB edge is relevant for the interpretation of the results.

## VI. RESULTS AND DISCUSSION

Results of optically measured MSB edges together with 2D MPB simulations based on hole radii extracted from SEM micrographs are shown in Fig. 9(a). The MSB spectral positions show a good agreement between measurements and simulations. Their absolute location depends on the exact fill ratios and therefore leads to significant differences between

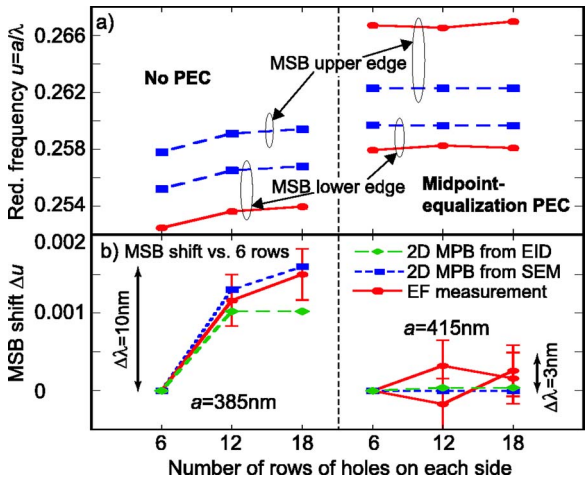


FIG. 9. (Color online) (a) Spectral location of the MSB edges computed with 2D MPB simulations with hole radii extracted from SEM micrographs (blue squares) and optical measurements (red ellipses). (b) Spectral shift of the MSB edges with respect to the six rows PECmeter determined from optical measurements (red ellipses), 2D MPB simulations with hole radii extracted from SEM micrographs (blue squares) and from EID simulations (green diamonds). Error bars for the measured MSB shifts correspond to an uncertainty of $\Delta\lambda=1$ nm in the determination of the MSB edges.

midpoint-equalization corrected and uncorrected waveguides, but which can be eliminated with a simple design bias.

We now focus our analysis on the relative shift of the MSB of 12 and 18 row waveguides with respect to PECmeters with six rows. The results are shown in Fig. 9(b). For the case of no PEC with $a=385$ nm, an excellent agreement can be seen between measured and simulated shifts. Further, EID simulations do predict nearly the same shift between 6 and 12 rows structures, but do not reproduce the experimentally observed considerably smaller shift between 12 and 18 rows structures. This is likely caused by a slight underestimation of the electron backscatter range $\beta$. Indeed, its determination relies on strongly overexposed doughnut-shaped features[25] which in turn induce charging effects in the $SiN_x$ hard mask.[21]

The MSB position of midpoint-equalization corrected PECmeters is well resolved. According to MPB simulations based on hole radii extracted from SEM micrographs as well as on EID simulations, the MSB shift is not expected to depend on the number of rows. This is in good agreement with the optical measurements which show unchanged positions of the MSB edges within the tolerance margins of the measurement. Well within the error margins, a slight increase of the MSB edges spectral positions can be recognized. This minute effect can be interpreted as the consequence of the underestimated electron backscatter range $\beta$ in combination with the limited accuracy of the midpoint-equalization PEC for small circles.[9] Nevertheless, we can state that the midpoint-equalization PEC achieves a near-to-perfect correction which manifests itself in a vanishingly small shift of the MSB.

As a last point we would like to briefly mention that the PECmeter method could also be used to accurately measure the proximity parameters. For this, however, the beam broadening parameter $\alpha$ should be known from a point exposure[26] or dose variation[9] measurement. The shift of the MSB of an uncorrected W3 for $N$ rows along the waveguide has to be measured for $N=6-18$ rows and the associated change in hole radius can be determined with, e.g., MPB. EID simulations then enable to find the proximity parameters $\beta$ and $\eta$ which give the best agreement with the changes in hole radius depending on $N$ the number of rows of holes along the waveguide. This procedure is somewhat tedious compared to, e.g., the doughnut technique[25] but suffers much less from charging effects of insulating substrates.

## VII. CONCLUSION

Our optical end-fire transmission measurements of the spectral shift of the W3 waveguides mini stop band convincingly showed that proximity effects during EBL patterning have a significant impact on the optical properties of photonic crystal-based devices. PEC is therefore required to suppress the dependence of optical characteristics on the PPC device extension. The introduced PECmeter method was shown to be a very sensitive tool to confirm the effectiveness and accuracy of PEC. Applied to fabricated devices, this

method demonstrated the near-to-perfect proximity-effects correction achieved with the midpoint-equalization method.

As a strategy to further improve the design, we would suggest to use, e.g., 6, 10, 14, and 18 rows of holes on each side of the waveguide and increased fill ratios as well as smaller lattice constants to enhance the influence of proximity effects. When applied to the W1 mode cutoff, which can be accurately located in the case of membrane-type PPC waveguides, this method would be well suited to determine changes of average hole diameters along the waveguide in the subnanometer regime.

## ACKNOWLEDGMENTS

This work was carried out in the framework of the Swiss National Science Foundation program, NCCR Quantum Photonics. The samples were fabricated at the FIRST Center of Micro- and Nanoscience of the ETH Zurich in the framework of the Nanostructuring Platform of the European ePiXnet network of excellence on photonic integrated circuits. The authors acknowledge E. Gini (FIRST) for the epitaxy, O. Homan (FIRST) for technical support and K. Rauscher and P. Ma for help in the early stages of the experiment.

[1] *Photonic Crystals: Physics, Fabrication and Applications*, edited by K. Inoue and K. Ohtaka (Springer, Berlin, 2004).
[2] M. Notomi, K. Yamada, A. Shinya, J. Takahashi, C. Takahashi, and I. Yokohama, Phys. Rev. Lett. **87**, 253902 (2001).
[3] B. S. Song, S. Noda, T. Asano, and Y. Akahane, Nat. Mater. **4**, 207 (2005).
[4] H. Takano, B. S. Song, T. Asano, and S. Noda, Appl. Phys. Lett. **86**, 241101 (2005).
[5] R. Wüest, P. Strasser, M. Jungo, F. Robin, D. Erni, and H. Jäckel, Microelectron. Eng. **67–68**, 182 (2003).
[6] A. S. Gozdz and P. S. Lin, Microelectron. Eng. **9**, 529 (1989).
[7] F. Robin, L. O'Faolain, G. Stark, R. Wüest, P. Strasser, K. Rauscher, A. Rampe, T. F. Krauss, and H. Jäckel, in Proceedings of the Photonic & Electromagnetic Crystal Structures-VI Conference, Crete, edited by C. M. Soukoulis (2005).
[8] E. Dulkeith, S. J. McNab, and Y. A. Vlasov, Phys. Rev. B **72**, 115102 (2005).
[9] R. Wüest, F. Robin, C. Hunziker, P. Strasser, D. Erni, and H. Jäckel, Opt. Eng. **44**, 043401 (2005).
[10] M. Skorobogatiy, G. Begin, and A. Talneau, Opt. Express **13**, 2487 (2005).
[11] K. Hennessy, C. Reese, A. Badolato, C. F. Wang, A. Imamoglu, P. M. Petroff, and E. Hu, J. Vac. Sci. Technol. B **21**, 2918 (2003).
[12] N. Ikeda, Y. Sugimoto, Y. Tanaka, K. Inoue, H. Oda, Y. Watanabe, and K. Asakawa, Semicond. Sci. Technol. **22**, 149 (2007).
[13] http://jdj.mit.edu/mpb
[14] S. G. Johnson and J. D. Joannopoulos, Opt. Express **8**, 173 (2001).
[15] M. Qiu, Appl. Phys. Lett. **81**, 1163 (2002).
[16] Y. Vlasov, M. O'Boyle, H. Hamann, and S. J. McNab, Nature (London) **438**, 65 (2005).
[17] L. O'Faolain *et al.*, in 32nd International Conference on Micro- and Nano-Engineering, edited by F. Prez-Murano (2006), Vol. 32.
[18] G. P. Watson, L. A. Fetter, and J. A. Liddle, J. Vac. Sci. Technol. B **15**, 2309 (1997).
[19] T. H. P. Chang, J. Vac. Sci. Technol. **12**, 1271 (1975).
[20] R. Wüest, Dissertation, ETH Nr. 17146, Electrical Engineering, ETH Zurich, Zurich, Switzerland, 2007.
[21] R. Wüest, P. Strasser, F. Robin, D. Erni, and H. Jäckel, J. Vac. Sci. Technol. B **23**, 3197 (2005).
[22] P. Strasser, R. Wüest, F. Robin, D. Erni, and H. Jäckel, J. Vac. Sci. Technol. B **25**, 387 (2007).
[23] R. Ferrini, D. Leuenberger, M. Mulot, M. Qiu, J. Moosburger, M. Kamp, A. Forchel, S. Anand, and R. Houdre, IEEE J. Quantum Electron. **38**, 786 (2002).
[24] G. Stark, F. Robin, R. Wüest, D. Erni, H. Jäckel, A. Christ, and N. Kuster (unpublished).
[25] L. Stevens, R. Jonckheere, E. Froyen, S. Decoutere, and D. Lanneer, Microelectron. Eng. **5**, 141 (1986).
[26] S. A. Rishton and D. P. Kern, J. Vac. Sci. Technol. B **5**, 135 (1987).